European Journal of Radiology 118 (2019) 138–146

Contents lists available at ScienceDirect

European Journal of Radiology

journal homepage: www.elsevier.com/locate/ejrad

Research article

Diagnostic evaluation of diffusion kurtosis imaging for prostate cancer: Detection in a biopsy population

Kai Ding[a,1], Yong Yao[b,1], Yun Gao[a], Xudong Lu[a], Hongwei Chen[a], Qunfeng Tang[a], Chenchen Hua[a], Ming Zhou[a], Xinnong Zou[a], Qihua Yin[a,*]

[a] Department of Radiology, The Affiliated Wuxi People's Hospital of Nanjing Medical University, No.299,Qingyang Road, Wuxi, 214000, Jiangsu Province, China
[b] Department of ophthalmology, The Affiliated Wuxi People's Hospital of Nanjing Medical University, No.299, Qingyang Road, Wuxi, 214000, Jiangsu Province, China

ARTICLE INFO

Keywords:
Magnetic resonance imaging
Diffusion-weighted imaging
Diffusion kurtosis
Prostate cancer
Gleason score

ABSTRACT

Purpose: To prospectively assess the feasibility of diffusional kurtosis (DK) imaging for distinguishing prostate cancer(PCa) from benign prostate hyperplasia (BPH) in comparison with standard diffusion-weighted (DW) imaging, as well as low-from high-grade malignant regions.

Materials and methods: 147 consecutive patients with suspected PCa underwent multi-parametric 1.5-TMR. Diffusion kurtosis imaging was acquired with with 5 b values (0,600,800,1600,and 2400sec/mm2).Region of interest (ROI)-based measurements were performed on ADC, D, and K map by two radiologists. Data were analyzed by using mixed-model analysis of variance and receiver operating characteristic curves. Correlations among the three parameters (ADC,D and K) in all patients, and correlations between three parameters with the tumor Gleason score (GS) in PCa group were analyzed using Pearson's correlation coefficient in peripheral zone (PZ) and transiton zone(TZ).

Results: 58 patients were proved with PCa (9 GS 3 + 3[PZ/TZ = 4/5], 49 GS ≥ 7 [PZ/TZ = 26/23]), and 89 patients were with BPH. ADC,D and K were able to distinguish benignance from tumor tissue both in PZ and TZ ($P < 0.01$), but performed poorly in neither differentiating low-(GS 3 + 3) from high-grade (GS ≥ 3 + 4) disease, nor GS(3 + 4) from GS(4 + 3).There was a weak correlation between the GS and ADC, D (PZ:ADC r = -0.113, D r = -0.139; TZ:ADC r = -0.104,D r = -0.103), while a moderate correlation between the GS and K(PZ:K r = 0.492; TZ:K r = 0.433, $P < 0.01$).K had significantly greater area under the curve for differentiating PCa from BHP than ADC both in PZ and TZ.

Conclusion: DK model may add value in PCa detection and diagnosis, but none can differentiate low-from high-grade PCas (including GS = 3 + 4 from GS = 4 + 3).

1. Introduction

Prostate cancer (PCa) is the second most common cancer among men, and its incidence rate invariably remains high in many countries worldwide [1]. PCa is the second leading cause of cancer death among men in 2012 [2].

The most popular method to a diagnosis of initial PCa is used by prostate specific antigen(PSA) testing, but it is still controversial due to considerable overdiagnosis and overtreatment [3]. Patients with benign prostatic hyperplasia(BPH), as an example, may also demonstrate elevated PSA level [4].

At present, the standard procedure to make a diagnosis of this disease depends on the systematic transrectal ultrasonography(TRUS)-guided biopsy, but it is invasive with possible unpleasant adverse effects and is prone to incorrect cancer localization and inaccurate Gleason score [5,6].Therefore, there is an urgent clinical need for improved tests for PCa diagnosis.

Multiparametric magnetic resonance imaging (MRI) manifests a great promise for the diagnosis of PCa. Traditional T_2-weighted MR imaging (T_2WI) provides tissue's anatomic information but can't precisely discriminate PCa from other benign diseases such as prostatitis and BPH [7]. Diffusion-weighted imaging (DW), MR spectroscopy and dynamic contrast-enhanced (DCE) MR imaging possess the potential to complement T_2WI [8,9]. Of all MR imaging modalities, diffusion-weighted imaging (DWI) is with its unique sensitivity to the microscopic structure of the tissue that influences tissue-water mobility.

* Corresponding author.
E-mail addresses: 13771450539@139.com (K. Ding), yinqihuaphd@163.com (Q. Yin).
[1] These authors contributed equally to this work.

https://doi.org/10.1016/j.ejrad.2019.07.009
Received 12 May 2019; Received in revised form 12 June 2019; Accepted 8 July 2019

Hence, DWI offers great potential value as a noninvasive diagnostic probe for cancer pathology.

Most previous studies have used a simple monoexponential model to describe signal decay with a range of increasing b-values. Apparent diffusion coefficient(ADC) obtained from DWI is characteristically lower in PCas than that in benign prostate tissues [10–12].The standard DWI model is that this approach assumes Gaussian behavior of water diffusion. However, signal decay is no longer monoxeponential with b-values, as demonstrated by a number of studies [13,14]. Diffusion kurtosis(DK) imaging, as an extension of traditional DW imaging, treats water diffusion as non-Gaussian in behavior and can better describe complex tissue microstructure [15–17].This technique provides a measure of the excess DK of tissue, which quantifies the deviation of tissue diffusion from a Gaussian pattern, as well as a diffusion coefficient that is corrected to account for this non-Gaussianity.

The purpose of this study is to prospectively assess the feasibility of the DK imaging model for distinguishing PCa from BPH in comparison with a standard DW imaging model, by using biopsy as the reference standard.

2. Material and methods

2.1. Patients

This study was approved by our institutional review board with a waiver of the requirement for written informed consent. Between May 2016 and October 2018, a total of 204 consecutive male patients (mean age:58.1 years; age range:53–88 years) with suspected PCa were referred for MR imaging. Patients with elevated serum PSA level (range, 1.28–5637.9 ng/mL) were included in this study. All cases were reviewed by a multidisciplinary team, including radiologists, urologists, and oncologists, and all the clinical information was available prior to the decision to undertake TRUS-guided biopsy or radical prostatectomy.

The inclusion criteria were as follows (Fig.1):(i)DICOM datasets with a multiple b-value DWI sequence; (ii)image quality without significant artifacts;(iii)without any prior treatment such as an endocrine therapy and/or a radiation treatment;(iv)definite pathological records and clinical records. Of these, 57 patients were excluded, a final cohort of 147 patients remained (mean age, 69.4years ± 8.5[sd]), and the mean preoperative prostate-specific antigen level was 10.5 ng/mL (range 1.42–5637.9 ng/mL).

The MRIs were prospectively interpreted by one of two experienced uroradiologists in prostate MRI reporting experience (no less than 10 years). Images were analysed according to PI-RADS version described in PI-RADS version 2. Interpretation was based on a Likert scale: 1, no suspicious area; 2, cancer unlikely; 3, indeterminate; 4, cancer likely; 5, cancer highly likely [18,19]. A Likert score($\geq$3) was defined as the positive lesion.

2.2. MR imaging technique

All patients underwent prostate MRI with a 1.5-Tesla MR scanner (Magnetom Aera; Siemens Healthcare, Erlangen, Germany) by using a 48-channel body-coil phased array for excitation and signal reception. Image acquisition details were summarized in Table 1 (standard DWI, b values = 0, 800 s/mm^2; DKI, five b-values = 0, 600,800, 1600 and 2400s/mm^2).

2.3. Prostate biopsy

All biopsies (134 cases) and prostatectomy patients (13 cases) were performed after MRI. TRUS-guided biopsies, performed by two urologists with 6 years' experience of transperineal biopsy using 18-Gneedles, were obtained in each case. Targets were prospectively drawn referring to T_2W as primary and ADC as secondary source images. For the targets, two or three biopsy cores were taken.

Each sample was histologically analyzed by two experienced genitourinary pathologists (10 and 15 years of experience, respectively) who were blinded to the MRI data. The criteria for the dominant lesion was the most aggressive focus for that patient (on the basis of Gleason

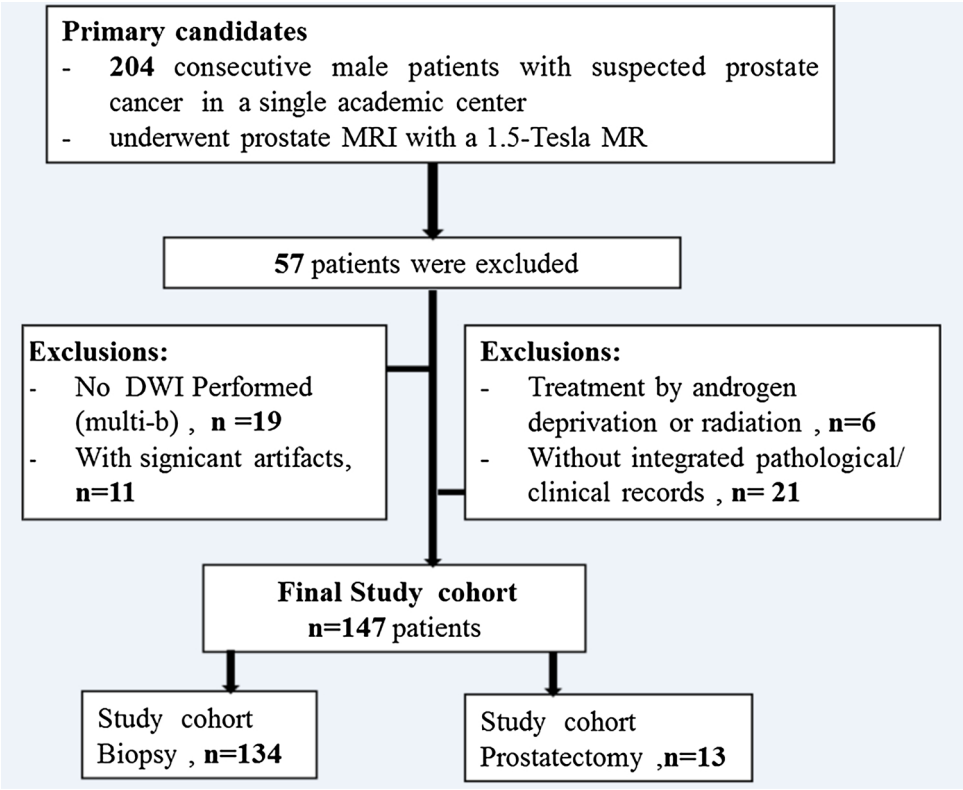

Fig. 1. Flow chart of patient population in current study.

Table 1
MR Image Acquisition Parameters.

Sequence, Imaging Plane and Sequence Type	TR (ms)	TE (ms)	ST (cm)	FOV (mm)	Matrix (cm)	PIF (n)	SA (n)	ISG (mm)
Axial T_1-weighted turbo spin echo imaging	500	8.6	3	200 × 200	320 × 240	2	2	0
Axial T_2-weighted turbo spin-echo imaging	4970	112	3	200 × 200	320 × 240	2	2	0
Coronal T_2-weighted turbo spin-echo imaging	6510	93	3	250 × 250	320 × 272	2	2	0.5
Sagittal T_2-weighted turbo spin-echo imaging	3860	93	3	250 × 250	320 × 240	2	2	0.9
Axial DWI fat suppressed single-shot spin-EPI	3100	52	3	258 × 258	192 × 133	2	2	0
Axial DKI fat suppressed single-shot spin-EPI	3100	52	3	258 × 258	192 × 133	2	6	0

Note.—EPI = Echo planar imaging, **TR** = Repetition time, **TE** = Echo time, **ST** = Section thickness, **FOV** = Field of view, **PIF** = Parallel imaging factor, **SA** = Signals acquired, **ISG** = Intersection gap.
DKI was acquired by using three orthogonal motion-probing gradient directions separately with the following b values (0,600,800,1600,and 2400sec/mm^2). For acquisition of standard DWI, b values were of 0 and 800 s/mm^2.

score[GS]). All biopsies were Gleason-graded by a specialist uropathologist, following ISUP 2005 recommendations [20].

2.4. Analysis of ADC and DKI data

The primary datasets were transferred to a personal computer and were processed by using previously described in house software programmed in Matlab **(** MathWorks, Natick,Mass) [21].

The software performs a voxel-by-voxel analysis that fits signal intensities (SI) from the DWI sequence as a function of b value by using the equation: $\mathbf{S = S_0\ exp(-b{\cdot}D + b^2{\cdot}D^2{\cdot}K/6)}$.Here the K is a phenomenological parameter, providing excellent mathematical fitting of the SI decay plot at very high b-values [22]. The K is on behalf of the excess kurtosis compared with a monoexponential model; K equals 0 signifying a perfectly Gaussian diffusion, and a larger K represents greater deviation of diffusion from perfectly Gaussian behavior. D is a corrected ADC that accounted for this non-Gaussianity.

The standard ADC is also calculated for each voxel by using a conventional monoexponential model with the equation $\mathbf{S = S_0{\cdot}exp(-b{\cdot}ADC)}$. Therefore, the software produces three separate parametric maps (ADC,D, and K)for each patient. We used b = 0 images and T_2WI images as an anatomical reference and drew regions of interest (ROIs) manually. The hypointense foci on T_2WI should be carefully included, and a great attention was paid to avoid hemorrhage (T_1WI may offer great potential value), necrosis, or calcification.

During the review, two distinct regions (Transition Zone [TZ] and Peripheral Zone[PZ]) on the parametric maps for each case were identified by radiologists, which manifested the most abnormal signal intensity in terms of a visual reduction in ADC or D or a visual elevation in K. The ROIs were drawn by two experienced radiologists in prostate imaging in consensus.

The ROI was chosen to ensure the area, as closely as feasible, histopathologically confirmed by targeted biopsy (or whole prostatectomy).The ROI was subsequently transferred to DKI parametric map and ADC map to calculate the DKI parameters of D, K and ADC. The size of ROIs (mean,0.43 ± 0.12cm^2; range,0.27–1.15 cm^2) was separately traced around the margin of each identified region. For DKI, the noise-only images were used to reduce and partially compensate for noise-floor bias. Measurement was repeated three times and the mean value for the ROIs was recorded (Figs.2,3 .)

2.5. Statistical analysis

Differences between BPHs and PCas in the parameters (ADC,D and K)were assessed using a mixed model analysis of variance (ANOVA) with patients as a random effect, and tumor grades(low, imtermeidate/high) both in the PZ and TZ. To assess supplementary information provided by the non-Gaussian model, Pearson correlation coefficients were calculated to assess relationships among the three parameters (ADC,D and K) in all patients, and between three parameters with the tumor GS. In addition, receiver operating characteristic (ROC) analyses were performed to evaluate the diagnostic performance of the parameters to discriminate PCas from BHPs.

Interobserver agreement analysis with k statistic was performed to determine consistency between the two radiologists for detection of lesion for the different MR imaging modalities (ADC, D and K map). A k value of 0-0.19 was considered poor agreement; 0.20–0.39, fair agreement; 0.40–0.59, moderate agreement; 0.60–0.79, substantial agreement; and 0.80–1.00, excellent agreement. The reproducibility of K as compared to ADC in diagnosis efficiency was assessed by using the discrepancies based on Bland Altman plots.

Comparisons were two sided and considered statistically significant when $P < 0.05$. Statistical analyses were performed by using software MedCalc version 12.5(MedCalc Software,Ostend, Belgium).

3. Results

3.1. Biopsy findings

On the basis of histopathologic examination, the final pathology of dominant lesion was identified as PCa in 58 patients. The mean postoperative Gleason score of the patients in this work was 8(range 6 − 9) including the peripheral zone (PZ) and in the transition zone (TZ).9 patients were with a Gleason score of 6 (9 Gleason 3 + 3 lesions, TZ vs. PZ = 5/4), and 49 patients were with a Gleason score greater than or equal to 7 (9 Gleason 3 + 4 lesions[TZ vs.PZ = 5/4], 11 Gleason 4 + 3 lesions [TZ vs.PZ = 6/5], 10 Gleason 4 + 4 lesions [TZ vs.PZ = 4/6], 10 Gleason 4 + 5 lesions [TZ vs.PZ = 4/6], and 9 Gleason 5 + 4 lesions [TZ vs.PZ = 4/5]). And the remainging 89 patients were diagnosed as BHPs (TZ vs.PZ = 68/21)

3.2. Kurtosis metrics

A summary of the metrics ADC,D, and K was demonstrated(Table 2 and Fig.4). All values were presented with Mean ± SD(standard deviation).

For all measured parameters, there was a significant difference between the BPH group and the tumor group (PZ and TZ, all $P < 0.01$). The ability of the parameters to distinguish low (GS 3 + 3) from intermediate/high-grade group high-grade (GS ≥ 7) was assessed, and GS 3 + 4 vs. GS 4 + 3 was also did. All measured parameters were poor at separating low-and intermediate/high-grade for both PZ (p = 0.16-0.78) and TZ (p = 0.25-0.53), and GS 3 + 4 vs.GS 4 + 3 (PZ, p = 0.23-0.82; TZ, p = 0.46-0.88). There was no significantly different in the value of three parameters between the PCa group (GS 3 + 3) and the PCa group (GS ≥ 7), neither between the PCa group of GS 3 + 4 and the PCa group of GS 4 + 3.

The values of ADC and D were both significantly lower in the PCa group (including GS 3 + 3, GS 3 + 4 GS 4 + 3 and GS ≥ 7) than those of the BPH group (PZ,ADC:0.76–0.89 ± 0.12–0.29 × 10^{-3} mm^2/s vs.

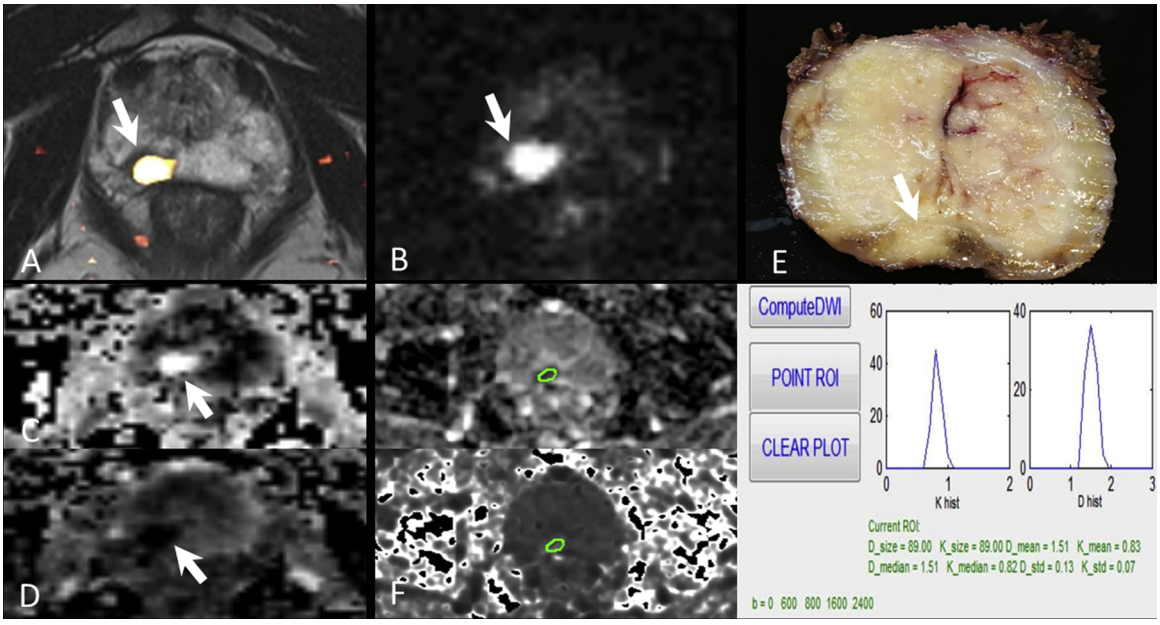

Fig. 2. A 73-year-old man with Gleason 9 (4 + 5) prostate cancer in the right midgland PZ at a whole prostatectomy biopsy. ROI was manifested on **C** and **D**. The lesion was manifested in the right midgland PZ (solid arrow). **A.** Axial T_2WI, and the boundary of the tumor was determined on fusional T_2WI and K map. **B.** DWI at b = 800, constructed by using a standard Gaussian model, and **C**. corrected diffusion coefficient(or D map). **D**. K map. **E.** Tissue processing of the resected specimen. **F.** DKI-processing.

$1.27 \pm 0.48 \times 10^{-3}\,mm^2/s$; D:1.07–$1.35 \pm 0.31$–$0.75 \times 10^{-3}\,mm^2/s$ vs. $2.03 \pm 0.74 \times 10^{-3}\,mm^2/s$, $P < 0.01$; TZ, ADC:0.81-0.93 ± 0.15-$0.22 \times 10^{-3}\,mm^2/s$ vs. $1.14 \pm 0.34 \times 10^{-3}\,mm^2/s$; D:0.98–$1.17 \pm 0.27$-$0.58 \times 10^{-3}\,mm^2/s$ vs. $1.64 \pm 0.51 \times 10^{-3}\,mm^2/s$, $P < 0.01$, respectively). K was significantly higher in the PCa group than those of the BPH group (PZ,0.71–0.94 ± 0.14–0.20 vs. 0.55 ± 0.12, $P < 0.01$; TZ,0.92–1.05 ± 0.13–0.26 vs. 0.68 ± 0.14, $P < 0.01$, respectively).

There was a weak correlation between the Gleason score and kurtosis parameters-ADC and D (PZ, ADC $r = -0.113$, D $r = -0.139$ $P > 0.05$; TZ, ADC $r = -0.104$,D $r = -0.103$, $P > 0.05$,respectively), while a moderate correlation between the Gleason score and kurtosis parameters-K(PZ, K $r = 0.492$ $P < 0.01$; TZ, K $r = 0.433$,$P < 0.01$,respectively). And there was also a negative correlation between parameters D and K (PZ, $r = -0.432^{\sim} - 0.760$,$p < 0.01$; TZ, $r = -0.360^{\sim} - 0.647$, $p < 0.01$), ADC and K (PZ, $r = -0.556^{\sim} - 0.720$, $p < 0.01$;TZ, r = -0.304~−0.566, $p < 0.01$). Meanwhile, ADC showed a strong overall correlation to D (PZ, r = 0.839–0.887,$p < 0.01$; TZ, r = 0.811–0.896, $p < 0.01$). Table 3

3.3. Summary of receiver operating characteristic analyses

The results of the receiver operating characteristic analyses of the ADC, D and K for distinguishing PCa from BPH were presented (Table 4 and Fig. 5).

There was significant difference between the AUC(area under curve)

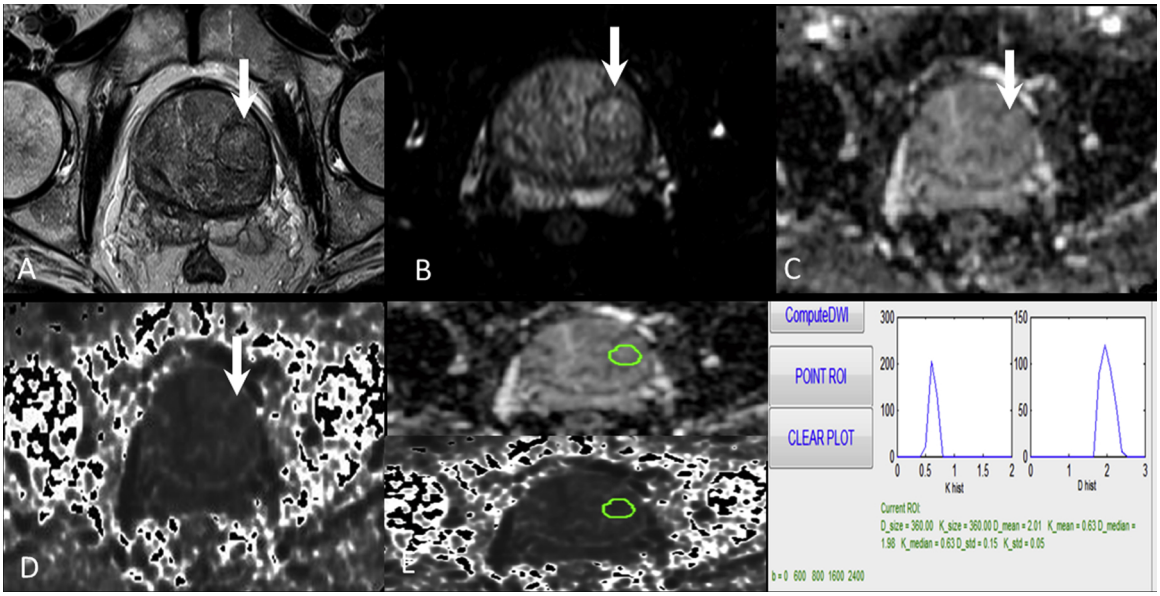

Fig. 3. A 66 year-in-old man with BPH, the lesion was manifested in the left midgland TZ (solid arrow),indicated by the white arrow: A. T_2WI; B. DW image at b = 0, constructed by using a standard Gaussian model; **C**. D map; **D.** K map. **E.** DKI-processing.

Table 2
ADC, D, and K for Various Tissue Types.

Parameter	BPH (PZ/TZ = 21/68)	PCa (N = 58)				$p^{\dagger}$	$p^{\ddagger}$	$p^{£}$
		(GS 3 + 3, PZ/TZ = 4/5)	(GS 3 + 4, PZ/TZ = 4/5)	(GS 4 + 3, PZ/TZ = 6/5)	(GS > 7, PZ/TZ = 16/13)			
ADC($\times 10^{-3}$ mm^2/s)								
PZ	1.27 ± 0.48	0.89 ± 0.20	0.78 ± 0.29	0.76 ± 0.12	0.79 ± 0.23	< 0.01	0.78	0.27
TZ	1.14 ± 0.34	0.93 ± 0.15	0.91 ± 0.18	0.87 < ± 0.20	0.81 ± 0.22	< 0.01	0.25	0.88
D($\times 10^{-3}$ mm^2/s)								
PZ	2.03 ± 0.74	1.35 ± 0.52	1.22 ± 0.75	1.07 ± 0.31	1.11 ± 0.48	< 0.01	0.36	0.23
TZ	1.64 ± 0.51	1.10 ± 0.27	0.98 ± 0.29	1.17 ± 0.58	1.13 ± 0.51	< 0.01	0.53	0.71
κ								
PZ	0.55 ± 0.12	0.71 ± 0.14	0.83 ± 0.20	0.89 ± 0.18	0.94 ± 0.18	< 0.01	0.16	0.82
TZ	0.68 ± 0.14	0.92 ± 0.26	1.05 ± 0.13	1.03 ± 0.17	1.02 ± 0.15	< 0.01	0.43	0.46

Note.—Data are means ± standard deviations. p < 0.05 is with statistically significant differences.
BPH = Benign prostate hyperplasia, **PCa** = Prostate cancer. **PZ** = Peripheral zone, **TZ** = Transition zone.**GS** = Gleason score. $P^{\dagger}$: P-value of **BHP** vs.**PCa;** $P^{\ddagger}$: P-value of **PCa(GS 3 + 3)** vs.**PCa (GS > 7),** $p^{£}$: P-value of **PCa(GS 3 + 4)** vs.**PCa (GS 4 + 3).**

among the three parameters in PZ (from 0.796 to 0.955, P < 0.01), and the AUC of ADC vs. K(0.753-0.928, P < 0.01), D vs. K in TZ (0.770–0.928, P < 0.01). But there was no statistical difference between the AUC of ADC vs. D in TZ (0.753–0.770, P = 0.65)

The AUC for ADC was 0.796 (0.702–0.871) with 95% confidence in PZ and 0.753 (0.064–0.835) in TZ, and using 1.285 × (10^{-3} mm^2/s) and 0.1.104 × (10^{-3} mm^2/s) as ADC cutoff value between benign and malignant lesions, in PZ the sensitivity and specificity was 100% and 61.8%; 8 cases (38.2%) were misclassified as PCa, and in TZ the sensitivity was 89.3% and specificity was 57.4%; 29 cases (42.7%) were misclassified as PCa.

The AUC for D was 0.861(0.776-0.922) with 95% confidence in PZ and 0.770 (0.673-0.850) in TZ, and using 2.048($\times 10^{-3}$ mm^2/s) and 1.398($\times 10^{-3}$ mm^2/s) as D cutoff value between benign and malignant lesions, the sensitivity and specificity was 96.7% and 60.3%; 8 cases (39.3%) were misclassified as PCa in PZ, and in TZ the sensitivity and specificity was 85.7% and 72.1%; 19 cases (27.9%) were misclassified as PCa.

For K, the AUC was 0.955 (0.894–0.987) with the 95% confidence interval in PZ and 0.928(0.857–0.971) in TZ, and using 0.695 and 0.871 as K cutoff value between benign and malignant lesions, the sensitivity and specificity was 90.0% and 92.7%; 2 cases (7.4%) were misclassified as BPHs in PZ, and in TZ the sensitivity and specificity was 82.1% and 92.7%; 2 cases (7.4%) were misclassified as BPHs.

3.4. Inter-observer reliability and the reproducibility of K as compared to ADC

There was fair to substantial agreement for detection of lesions (TZ, k = 0.41 for ADC, k = 0.64 for D, and k = 0.76 for K; PZ, k = 0.63 for ADC, k = 0.68 for D, and k = 0.81 for K).

In PZ, matching data difference of 51 cases was 0.245 ± 0.621(mean ± sd), 95%CI of limits of agreement was as follows: lower limit, −0.971, 95%CI(−1.271˜−0.671); upper limit,1.46, 95%CI(1.161 ˜1.762), and 3.9% (2/51) of the points was outside the 95%CI of mean of differences. Within the scope of it, the difference of maximum absolute value of the K and ADC detection value was 0.49, the result of two ways in diagnosis of prostatic lesion was with an average of 0.25. Meanwhile In TZ, matching data difference of 96 cases was 0.253 ± 0.479(mean ± sd), 95%CI of limits of agreement was as follows: lower limit, −0.687,95%CI(−0.854˜−0.521);

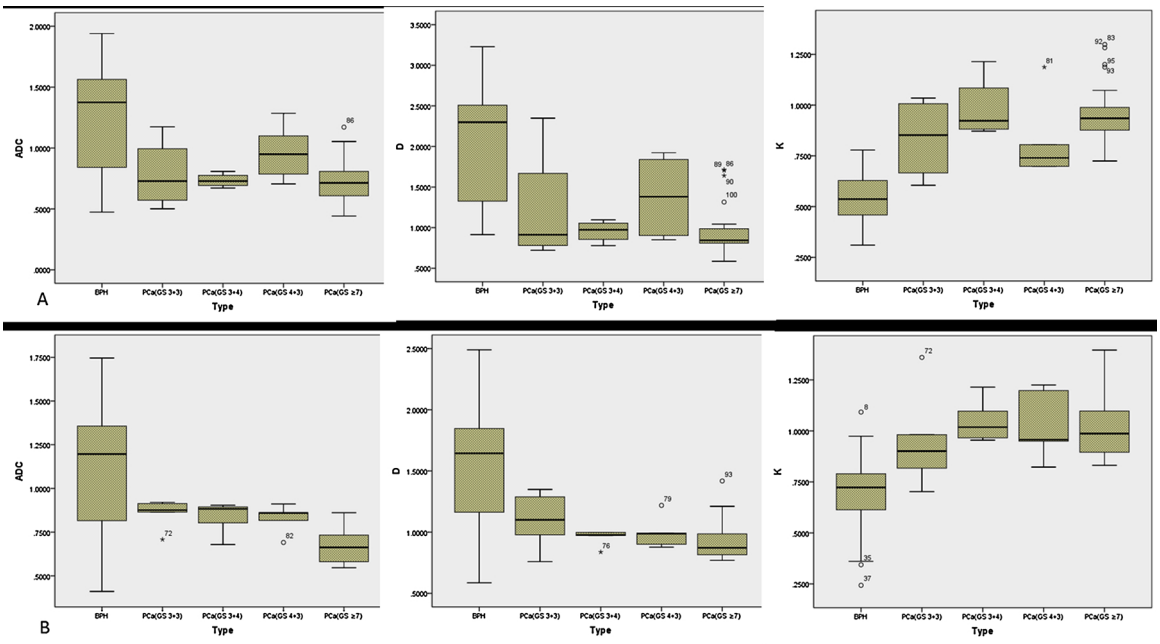

Fig. 4. Boxplot statistical distributions of ADC($\times 10^{-3}$ mm^2/sec), D ($\times 10^{-3}$ mm^2/sec) and K in BPH,PCa(GS3 + 3), PCa(GS3 + 4), PCa(GS4 + 3) and PCa ≥ 7 in the PZ and the TZ. A. PZ, B. TZ. The top and bottom of each box is the 25th and 75th percentile, respectively; line in the middle represents median value. Whiskers extend to the most extreme data points but are still within1.5 times the interquartile range from the top or bottom of the box; outliers beyond this range are represented by °.

Table 3
Correlation between assessed metrics (Pearson's Rho).

Comparators	Peripheral Zone (*r*)				Transition Zone (*r*)			
	PCa(95% CI)	BPH(95% CI)	BPH + PCa(95% CI)	$P^{\dagger}$	PCa(95% CI)	BPH(95% CI)	BPH + PCa(95% CI)	$P^{\ddagger}$
ADC vs. D	0.887(0.777~0.945)	0.872(0.801~0.919)	0.893(0.841~0.927)	< 0.01	0.811(0.629~0.909)	0.894(0.834~0.934)	0.886(0.834~0.923)	< 0.01
ADC vs. K	−0.720(-0.856~-0.492)	−0.556(-0.702~-0.367)	−0.691(-0.783~-0.572)	< 0.01	−0.566(-0.776~-0.246)	−0.304(-0.563~-0.212)	−0.329(-0.497~-0.138)	< 0.01
D vs. K	−0.760(-0.878~-0.556)	−0.432(-0.608~-0.217)	−0.713(-0.799~-0.601)	< 0.01	−0.647(-0.822~-0.362)	−0.360(-0.616~-0.223)	−0.477(-0.619~-0.307)	< 0.01
ADC vs. GS	−0.113(-0.458~0.210)	/	/	> 0.05	−0.104(-0.477~0.231)	/	/	> 0.05
D vs. GS	−0.139(-0.440~0.233)	/	/	> 0.05	−0.103(-0.419~0.242)	/	/	> 0.05
K vs. GS	0.492(0.230~0.708)	/	/	< 0.01	0.433(0.211~0.658)	/	/	< 0.01

Note.—Mean values listed, interquartile range in parentheses; $p < 0.05$ is with statistically significant differences.
PCa = Prostate cancer, **BPH** = Benign prostate hyperplasia, **GS** = Gleason score, **r** = Pearson correlation coefficient, **CI** = confidence interval. $P^{\dagger}$: P-value in Peripheral Zone; $P^{\ddagger}$: P-value in Transition Zone.

upper limit,1.193, 95%CI(1.1027~1.360), and 2.0% (2/96) of the points was outside the 95%CI of mean of differences. Within the scope of it, the difference of maximum absolute value of the K and ADC detection value was 0.50, the result of two ways in diagnosis of prostatic lesion was with an average of 0.25.(Fig.6)

4. Discussion

In this study we assessed the potential added value of non-Gaussian diffusion kurtosis imaging to conventional mpMRI sequences for the detection of prostate cancer in a biopsy (using targeted transperineal biopsy) or whole prostatectomy as the reference standard. All three measured parameters were able to distinguish benign from tumor tissue both in PZ and TZ($P < 0.01$), but performed poorly at neither differentiating low-(GS 3 + 3) from high-grade (GS ≥ 3 + 4) disease, nor GS (3 + 4) from GS(4 + 3). ADC and D manifested a weak correlation with GS both in PZ and TZ($P > 0.01$), interesting K demonstrated a moderate correlation with GS($P < 0.01$). Both in PZ and TZ, ADC and D demonstrated a strong negative correlation with K within tumors, and meanwhile ADC manifested a positive correlation with D.

Many previous studies have pay attention to the ability of DKI to differentiate tumor grade compared to standard diffusion-weighted imaging with mono-exponential modeling.

ADC was demostrated to decrease as tumor Gleason grade increases, Albeit with a degree of overlap in values between tumor grades [23,24]. However, the concordance between ADC and Gleason grade has recently been questioned [25], with the demonstration that Gleason 3 + 3 tumors can have low ADC values [26]. Our study support this opinion, the ADC values do not manifest a Linear gradient among PCas (GS = 3 + 3, GS 3 + 4, GS 4 + 3 and GS > 7). We have a hypothesis this may relate to the relatively small sample size.

DKI parameters have repeatedly been manifested to distinguish benign from tumor tissue, and suggested that the kurtosis metric K outperforms ADC for differentiating low-and high-grade tumors [27,28]. Our results did not entirely conform to these views, Three measured parameters could distinguish benign from tumor both in PZ and TZ($p < 0.01$), but they neither differentiate low grade (GS = 3 + 3) from high grade (GS > 3 + 4, p = 0.16-0.78), nor GS = 3 + 4 from GS = 4 + 3(p = 0.23-0.88) both in PZ and in TZ. We conjecture that cellularity is partly contributing to these metrics, whilst their divergent values are attributing to other factors.

As noted previously, stromal, epithelial and glandular compartments may induce multi-exponential diffusion response in prostate tissue [29]. Benign prostate tissues possess rich glandular units and glandular tubes, and acini are radially arranged along the urethra, and as a result this branching duct-acinar glandular architecture retains a high freedom of water diffusion [30]. In comparison, PCa cells proliferation and hence cellularity rise, consequently decreasing extracellular space; nucleoplasm ratio increases and intercellular space constricts. These disrupted duct-acinar structures impede water diffusion, thus leading to a decreased molecular motion of water. Additionally at higher Gleason grades, the glandular structure of the prostate is progressively disrupted with increased cellularity and a reduction in the stromal matrix and luminal space [31].

Due to increased cellular density, higher-grade prostate cancer is expected to result in an increased number of intracellular bound water molecules [32]; however, this is counteracted by a breakdown of the normal extensive extracellular matrix [33].This increased heterogeneity can therefore contribute to explain a trend for higher K values in tumors. These competing processes may provide an explanation for the divergence between DWI and DKI in tumors. [34]

Recent studies have shown that DKI offers a method to evaluate the non-gaussian diffusion behavior in complex biological tissues in brain diseases, breast tumors and abdominal organs [35–37]. In particular, DKI can potentially augment conventional diffusion techniques for better tumor lesion characterization.

Table 4
Receiver Operating Characteristic Analysis of ADC, D, and K for Discriminating PCa from BPH.

Measure	AUC (95% CI)	Cutoff Value	Sensitivity(%)	Specificity(%)
ADC $\times 10^{-3}$mm/s				
PZ	0.796(0.702–0.871)	≤1.285	100%	61.8%
TZ	0.753(0.654–0.835)	≤1.104	89.3%	57.4%
D $\times 10^{-3}$mm/s				
PZ	0.861(0.776–0.922)	≤2.048	96.7%	60.3%
TZ	0.770(0.673–0.850)	≤1.398	85.7%	72.1%
K				
PZ	0.955(0.894–0.987)	> 0.695	90.0%	92.7%
TZ	0.928(0.857–0.971)	> 0.871	82.1%	92.7%

Note— Optimal threshold of each parameter was selected to maximize average of sensitivity and specificity. Data in parentheses are numbers used to calculate percentages.
K showed the greatest sensitivity and specificity for detecting PCa among three parameters. **AUC** = Area under the curve, **PCa** = Prostate cancer, **BPH** = Benign prostate hyperplasia.

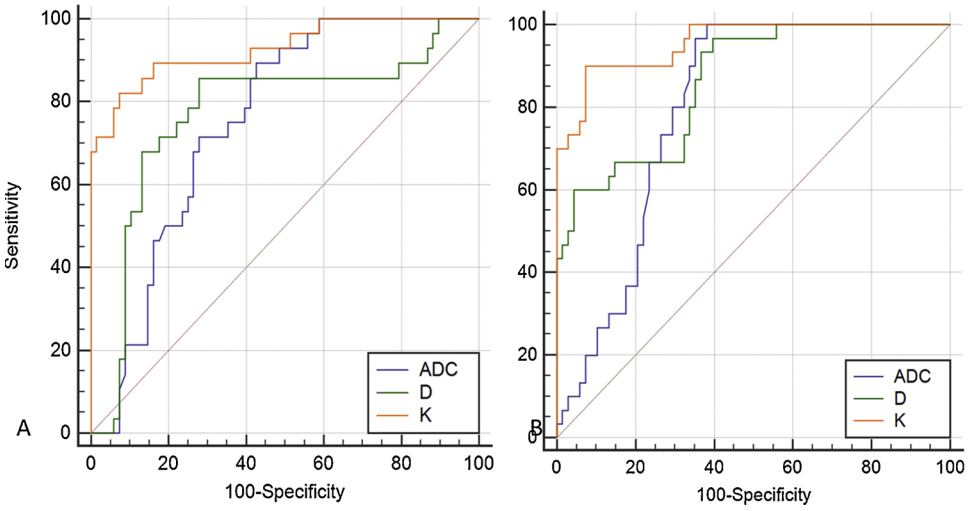

Fig. 5. Receiver operating characteristic curve for ADC,D and K values used as predictors of PCa in PZ (A) and TZ (B). There was significant difference between the AUC(area under curve) among ADC,D and K in PZ (from 0.796 to 0.955,P < 0.01), and in TZ the AUC of ADC vs. K(0.753-0.928, P < 0.01), D vs. K (0.770-0.928, P < 0.01). But there was no statistical difference between the AUC of ADC vs. D in TZ (0.753-0.770, P = 0.65). Gray line = chance diagonal.

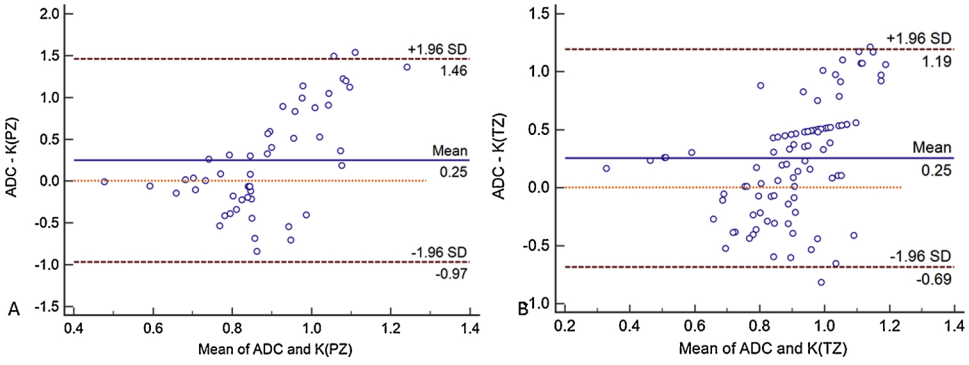

Fig. 6. Diffuse parameter: Difference (ADC-K) versus average of values measured by observer ADC and K with 95% limits of agreement. A. leisons in the PZ, **B.** lesions in the TZ. The upper and lower horizontal lines represent the upper and lower limits of the 95% agreement to this plot, the middle solid line represents the mean of the difference, and the dotted line represents the mean of the difference (Y = 0).

The results of ROC analysis were suggestive of significant difference in the AUC for detection of PCa by using the three metrics in PZ(P < 0.01). ADC noted the highest sensitivity(100%) and a high specificity, from this point of view, ADC either outperformed or performed similarly to K, we must acknowledged that ADC map is a convenient and effective tool for clinical routine application, but the use of K led to a higher specificity and lower percentage for misclassification than ADC and D did in benign and malignant prostatic lesions, indicating a better diagnostic performance (Table 4 and Fig. 5). While in TZ, there was no statistical difference between the AUC of ADC vs. D (P = 0.65). ADC and D were concordant in the sensitivity of detection than K did, similarly ADC was sufficient for tumor detection, but K also manifested a good differentiating diagnostic efficiency.

We speculate that the organizational complexity may account for this. Compared with the PZ, the tissue structure of lesions may be more complexity in TZ. Another explanation may be the longer echo time (TE) used in the DKI sequence to achieve the diffusion weighting, which reduces the intrinsic SNR of the D obtained using lower b-values [14]. ADC is derived by using a monoexponential fit that does not account for the deviation from a Gaussian distribution occurring at very high b values. K is associated with tissue complexity and may therefore reflect tissue microstructure [28]. Thus by our work, these are good grounds for believing that DKI may add valuable indications of microstructural changes to conventional diffusion techniques for the characterization of prostatic tumors.

Microcirculation-induced dephasing or intravoxel incoherent motion effects associated with tumor angiogenesis may lead to biexponential DW signal decay in prostatic tumor tissue at lower diffusion weighting (b < 200 s/mm^2) [38–40]. The perfusion component within tissues is, accounting for a dominant influence, more than diffusion,

and as a result, the obtained ADC is not only associated with pure diffusion [10].This mechanism should been considered in prostate cancer tissue [41,42],thus in our study the high b values was used to minimize microcirculation effects in favor of microstructural information. In the case of b-values higher than 2000sec/mm^2, the SNR decreases and image quality is often a concern, which may affect the accuracy of the results [29]. There was the range of b-values (0,600,800,1600, and 2400s/mm^2) in our work, low b-values (b < 600 s/mm^2) were not included to avoid perfusion as much as possible and a high b-value (b = 2400s/mm^2) was applied to ensure adequate imaging of kurtosis. This range was similar to that applied in the study by Rosenkrantz et al [13]. The SNR for DW images (b = 2400s/mm^2) obtained in our study was satisfactory. When high b-values were lower than 2500–3000 s/mm^2, the K was a phenomenological parameter, providing excellent mathematical fitting of the SI decay plot [22].

There are several limitations in our work. Firstly, compared to the more robust gold standard of prostatectomy, our targets biopsies were TRUS-guided prospectively depending on visual inspection of MRI (T_2WI and ADC) as source images, and these metrics for the match of cancerous sites between pathology and MRI, the placement of ROI within PCas and BPHs, may result in sampling error and a selection bias to the measurements and subsequently influence our observations [43]. This may have led to a bias towards lesions with restricted diffusion and low ADC, particularly within the PZ where this is considered the key diagnostic sequence. Secondly,in our examination the samples in the PCa group were relatively small, so that the role of DK imaging metrics was poor in assessment of high-and low-grade PCas, where further subdivision became necessary. At last, all of the PCas and BPHs on MRI were performed on 1.5 T scanner not 3.0 T, which was probably to lead to image quality degradation and inaccurate localization.

In conclusion, DKI can provide better changes of the cellularity, stromal matrix, and luminal space in BPH and PCa than ADC does. ADC and DKI readily distinguish benign tissue from tumor, but none of the parameters differentiate low-from high-grade PCas(including GS = 3 + 4 from GS = 4 + 3). And K demonstrates a greater relative specificity for PCa. Therefore, DKI may not only offer difference but potentially complementary information on the tumor microstructural complexity.

Funding

This study was funded by Key project in Wuxi People's Hospital (No. YT201317).

Declaration of Competing Interest

No conflict of interest exits in the submission of this manuscript, and manuscript is approved by all authors for publication. I would like to declare on behalf of my co-authors that the work described was original research that has not been published previously, and not under consideration for publication elsewhere, in whole or in part. All the authors listed have approved the manuscript that is enclosed.

Ethical approval

This study was approved by our institutional review board with a waiver of the requirement for written informed consent.

References

[1] M.M. Center, A. Jemal, J. Lortet-Tieulent, et al., International variation in prostate cancer incidence and mortality rates, Eur. Urol. 61 (2012) 1079–1092.
[2] O.W. Brawley, Trends in prostate cancer in the United States, J. Natl. Cancerral zone(PZ) and transiton zone(T Inst. Monogr. 45 (2012) 152–156.
[3] N. Pashayan, P. Pharoah, D.E. Neal, et al., PSA-detected prostate cancer and the potential for dedifferentiation–estimating the proportion capable of progression, Int. J. Cancer 128 (2011) 1462–1670.
[4] C.M.A. Hoeks, J.O. Barentsz, T. Hambrock, et al., Prostate cancer: multiparametric MR imaging for detection, localization, and staging, Radiology 261 (2011) 46–66.
[5] A. Rajinikanth, M. Manoharan, C.T. Soloway, et al., Trends in gleason score: concordance between biopsy and prostatectomy over 15 years, Urology 72 (2008) 177–182.
[6] S.W. Heijmink, H. van Moerkerk, L.A. Kiemeney, et al., A comparison of the diagnostic performance of systematic versus ultrasoundguided biopsies of prostate cancer, Eur. Radiol. 16 (2006) 927–938.
[7] J. Döpfert, A. Lemke, A. Weidner, et al., Investigation of prostate cancer using diffusion-weighted intravoxel incoherent motion imaging, Magn. Reson. Imaging 29 (2011) 1053–1058.
[8] J.J. Fütterer, S.W. Heijmink, T.W.J. Scheenen, et al., Prostate cancer localization with dynamic contrast-enhanced MR imaging and proton MR spectroscopic imaging, Radiology 241 (2006) 449–458.
[9] P. Kozlowski, S.D. Chang, E.C. Jones, et al., Combined diffusion-weighted and dynamic contrast-enhanced MRI for prostate cancer diagnosis—correlation with biopsy and histopathology, J. Magn. Reson. Imaging 24 (2006) 108–113.
[10] K. Yoshimitsu, K. Kiyoshima, H. Irie, et al., Usefulness of apparent diffusion coefficient map in diagnosing prostate carcinoma: correlation with stepwise histopathology, J. Magn. Reson. Imaging 27 (2007) 132–139.
[11] S.I. Jung, O.F. Donati, H.A. Vargas, et al., Transition zone prostate cancer: incremental value of diffusion-weighted endorectal MR imaging in tumor detection and assessment of aggressiveness, Radiology 269 (2013) 493–503.
[12] C.H. Tan, W. Wei, V. Johnson, et al., Diffusion-weighted MRI in the detection of prostate cancer: meta-analysis, Am. J. Roentgenol. 199 (2012) 822–189.
[13] A.B. Rosenkrantz, E.E. Sigmund, G. Johnson, et al., Prostate cancer: feasibility and preliminary experience of a diffusional kurtosis model for detection and assessment of aggressiveness of peripheral zone cancer, Radiology 264 (2012) 126–135.
[14] M.C. Roethke, T.A. Kuder, T.H. Kuru, et al., Evaluation of diffusion kurtosis imaging versus standard diffusion imaging for detection and grading of peripheral zone prostate Cancer, Invest. Radiol. 50 (2015) 483–489.
[15] H. Lu, J.H. Jensen, A. Ramani, et al., Three-dimensional characterization of nonGaussian water diffusion in humans using diffusion kurtosis imaging, NMR Biomed. 19 (2006) 236–247.
[16] J.H. Jensen, J.A. Helpern, MRI quantification of non-Gaussian water diffusion by Kurtosis analysis, NMR Biomed. 23 (2010) 698–710.
[17] J.H. Jensen, J.A. Helpern, A. Ramani, et al., Diffusional kurtosis imaging:the quantification of non-Gaussian water diffusion by means of magnetic resonance imaging, Magn. Reson. Med. 53 (2005) 1432–1440.
[18] J.O. Barentsz, J. Richenberg, R. Clements, et al., ESUR prostate MR guidelines 2012, Eur. Radiol. 22 (2012) 746–757.
[19] A.B. Rosenkrantz, S. Kim, R.P. Lim, et al., Prostate cancer localization using multiparametric MR imaging: comparison of Prostate Imaging Reporting and Data System (PI-RADS) and Likert scales, Radiology 269 (2013) 482–492.
[20] J.L. Epstein, Amin M.B. AllsbrookWCJr, et al., The 2005 international society of urological pathology (ISUP) consensus conference on Gleason grading of prostatic carcinoma, Diagn. Mol. Pathol. 29 (2015) 1228–1242.
[21] A. Tabesh, J.H. Jensen, B.A. Ardekani, et al., Estimation of tensors and tensor-derived measures in diffusional kurtosis imaging, Magn. Reson. Med. 65 (2011) 823–836.
[22] D. Le Bihan, Apparent diffusion coefficient and beyond: what diffusion MR imaging can tell us about tissue structure, Radiology 268 (2013) 318–322.
[23] T. Hambrock, D.M. Somford, H.J. Huisman, et al., Relationship between apparent diffusion coefficients at 3.0-T MR imaging and Gleason grade in peripheral zone prostate cancer, Radiology 259 (2011) 453–461.
[24] O.F. Donati, Y. Mazaheri, A. Afaq, et al., Prostate cancer aggressiveness: assessment with whole-lesion histogram analysis of the apparent diffusion coefficient, Radiology 271 (2014) 143–145.
[25] A. Chatterjee, G. Watson, E. Myint, et al., Changes in epithelium, stroma, and lumen space correlate more strongly with Gleason pattern and are stronger predictors of prostate ADC changes than cellularity metrics, Radiology 277 (2015) 751–762.
[26] O. Helfrich, P. Puech, N. Betrouni, et al., Quantified analysis of histological components and architectural patterns of Gleason grades in apparent diffusion coefficient restricted areas upon diffusion weighted MRI for peripheral or transition zone cancer locations, J. Magn. Reson. Imaging 46 (2017) 1786–1796.
[27] E.M. Lawrence, A.Y. Warren, A.N. Priest, et al., Evaluating prostate cancer using fractional tissue composition of radical prostatectomy specimens and pre-operative diffusional kurtosis magnetic resonance imaging, PLoS One 11 (2016) e0159652.
[28] C. Tamura, H. Shinmoto, S. Soga, et al., Diffusion kurtosis imaging study of prostate cancer: preliminary findings, J. Magn. Reson. Imaging 40 (2014) 723–729.
[29] R. Bourne, N. Kurniawan, G. Cowin, et al., 16 T Diffusion microimaging of fixed prostate tissue: preliminary findings, Magn. Reson. Med. 66 (2011) 244–247.
[30] A.B. Rosenkrantz, A.R. Padhani, T.L. Chenevert, et al., Body diffusion kurtosis imaging: basic principles, applications, and considerations for clinical practice, J. Magn. Reson. Imaging 42 (2015) 1190–1202.
[31] E.M. Lawrence, S.Y. Tang, T. Barrett, et al., Prostate cancer: performance characteristics of combined T2Wand DW-MRI scoring in the setting of template transperineal re-biopsy using MRTRUS fusion, Eur. Radiol. 24 (2014) 1497–1505.
[32] G. Jia, R. Abaza, J.D. Williams, et al., Amide proton transferMR imaging of prostate cancer: a preliminary study, J. Magn. Reson. Imaging 33 (2011) 647–654.
[33] Y. Takayama, A. Nishie, M. Sugimoto, et al., Amide proton transfer (APT) magnetic resonance imaging of prostate cancer:comparison with Gleason scores, MAGMA 29 (2016) 671–679.
[34] T. Barrett, M. McLean, A.N. Priest, et al., Diagnostic evaluation of magnetization transfer and diffusion kurtosis imaging for prostate cancer detection in a re-biopsy population, Eur. Radiol. 28 (2018) 3141–3150.

[35] J.F. Jansen, H.E. Stambuk, J.A. Koutcher, et al., Non-Gaussian analysis of diffusion-weighted MR imaging in head and neck squamous cell carcinoma: a feasibility study, AJNR Am. J. Neuroradiol. 31 (2010) 741–748.
[36] A. Christou, A. Ghiatas, D. Priovolos, et al., Accuracy of diffusion kurtosis imaging in characterization of breast lesions, Br. J. Radiol. 90 (2017) 20160873.
[37] A. Müller-Lutz, D. Blondin, Antoch G, et al; Diffusion kurtosis imaging of the human kidney: a feasibility study, Magn. Reson. Imaging 32 (2014) 413–420.
[38] S. Woo, J.M. Lee, J.H.J. Yoon, et al., Intravoxel incoherent motion diffusion-weighted MR imaging of hepatocellular carcinoma: correlation with enhancement degree and histologic grade, Radiology 270 (2014) 758–767.
[39] Y.Y. Yan, S. Hartono, T. Hennedige, et al., Intravoxel incoherent motion and diffusion tensor imaging of early renal fibrosis induced in a murine model of streptozotocin induced diabetes, Magn. Reson. Imaging 38 (2017) 71–76.
[40] E.E. Sigmund, G.Y. Cho, S. Kim, et al., Intravoxel incoherent motion imaging of tumor microenvironment in locally advanced breast cancer, Magn. Reson. Med. 65 (2011) 1437–1447.
[41] M. Valerio, C. Zini, D. Fierro, et al., 3T multiparametric MRI of the prostate: does intravoxel incoherent motion diffusion imaging have a role in the detection and stratification of prostate cancer in the peripheral zone? Eur. J. Radiol. 85 (2016) 790–794.
[42] F. Pesapane, F. Patella, E.M. Fumarola, et al., Intravoxel incoherent motion (IVIM) diffusion weighted imaging (DWI) in the periferic prostate cancer detection and stratification, Med. Oncol. 34 (2017) 35.
[43] C. Lanz, F. Cornud, F. Beuvon, et al., Gleason score determination with transrectal ultrasound-magnetic resonance imaging fusion guided prostate biopsies–are we gaining in accuracy? J. Urol. 195 (2016) 88–93.